PDGFRα signaling in the primary cilium regulates NHE1-dependent fibroblast migration via coordinated differential activity of MEK1/2–ERK1/2–p90^{RSK} and AKT signaling pathways

Ditte L. Clement[1], Sabine Mally[2], Christian Stock[2], Mette Lethan[3], Peter Satir[3], Albrecht Schwab[2], Stine F. Pedersen[1] and Søren T. Christensen[1,*]

[1]Department of Biology, University of Copenhagen, August Krogh Building, Universitetsparken 13, DK-2100 Copenhagen OE, Denmark
[2]Institute for Physiology II, Münster University, Robert-Koch-Str. 27b, 48149 Münster, Germany
[3]Department of Anatomy and Structural Biology, Albert Einstein College and Medicine, Jack and Pearl Resnick Campus, 1300 Morris Park Avenue, Forchheimer Building, Bronx, New York, NY 10461, USA
*Author for correspondence (stchristensen@bio.ku.dk)

Accepted 22 November 2012
Journal of Cell Science 126, 953–965

doi: 10.1242/jcs.116426

Summary

In fibroblasts, platelet-derived growth factor receptor alpha (PDGFRα) is upregulated during growth arrest and compartmentalized to the primary cilium. PDGF-AA mediated activation of the dimerized ciliary receptor produces a phosphorylation cascade through the PI3K–AKT and MEK1/2–ERK1/2 pathways leading to the activation of the Na^+/H^+ exchanger, NHE1, cytoplasmic alkalinization and actin nucleation at the lamellipodium that supports directional cell migration. We here show that AKT and MEK1/2–ERK1/2–p90^{RSK} inhibition reduced PDGF-AA-induced cell migration by distinct mechanisms: AKT inhibition reduced NHE1 activity by blocking the translocation of NHE1 to the cell membrane. MEK1/2 inhibition did not affect NHE1 activity but influenced NHE1 localization, causing NHE1 to localize discontinuously in patches along the plasma membrane, rather than preferentially at the lamellipodium. We also provide direct evidence of NHE1 translocation through the cytoplasm to the leading edge. In conclusion, signals initiated at the primary cilium through the PDGFRαα cascade reorganize the cytoskeleton to regulate cell migration differentially through the AKT and the MEK1/2–ERK1/2–p90^{RSK} pathways. The AKT pathway is necessary for initiation of NHE1 translocation, presumably in vesicles, to the leading edge and for its activation. In contrast, the MEK1/2–ERK1/2–p90^{RSK} pathway controls the spatial organization of NHE1 translocation and incorporation, and therefore specifies the direction of the leading edge formation.

Key words: Primary cilia, PDGFRα, MEK1/2–Erk1/2–p90^{RSK}, AKT, NHE1, Cell migration

Introduction

The primary cilium found on most mammalian and human cells is a signaling center for normal developmental and physiological processes in the body (Christensen et al., 2012; Goetz and Anderson, 2010; Satir et al., 2010; Wallingford and Mitchell, 2011). When ciliogenesis is abnormal or the signal transduction pathway does not function properly, often because specific receptors are not properly localized to the ciliary membrane, the result is a series of pathologies, now called ciliopathies, such as cystic kidney disease or a failure of tissue repair as in wound healing or cardiac remodeling (Christensen et al., 2008; Hildebrandt et al., 2011; Waters and Beales, 2011). In NIH3T3 and mouse embryo fibroblasts (MEFs), the receptor tyrosine kinase, platelet-derived growth factor receptor alpha (PDGFRα) is upregulated during ciliogenesis and traffics to the ciliary membrane. When a ligand is present, the receptor at the cilium dimerizes and signals via a phosphorylation cascade to molecules controlling cell division, migration and wound healing (Schneider et al., 2005; Schneider et al., 2009; Schneider et al., 2010). Both the PI3K–AKT and the MEK1/2–ERK1/2 pathways transduce the signal via unknown mechanisms. A suggested hypothesis is that downstream in the transduction pathway, vesicles containing the Na^+/H^+ exchange protein NHE1 move toward the leading edge of the cell (Schneider et al., 2009).

NHE1 is a key regulator of multiple cellular processes, including cell proliferation, survival and migration (Boedtkjer et al., 2012; Pedersen, 2006; Stock and Schwab, 2006). NHE1 localizes to the leading edge membrane of migrating cells as well as to adhesive/invasive structures such as invadopodial rosettes (Lagana et al., 2000; Lauritzen et al., 2012; Martin et al., 2011; Patel and Barber, 2005), anchors the actin cytoskeleton to the plasma membrane (Denker et al., 2000; Wu et al., 2004) and interacts with integrins (Yi et al., 2009). NHE1 expression is upregulated during quiescence concomitant with formation of the primary cilium (Schneider et al., 2009). The mechanisms by which NHE1 relocalizes to the leading edge upon fibroblast polarization and migration are unknown. While in platelets and lymphocytes, NHE1 does not appear to be acutely regulated by vesicular insertion (Dixon et al., 1987), recent studies have demonstrated NHE1 plasma membrane translocation in response to integrin activation in fibroblasts (Yi et al., 2009) and insulin stimulation in cardiomyocytes (Lawrence et al., 2010), the latter

in a PI3K-dependent manner. Both the PI3K–AKT and the MEK1/2–ERK1/2–p90^{RSK} signaling pathways have been implicated in the regulation of NHE1 activity, but the mechanisms involved are incompletely understood and conflicting evidence has been reported (Malo et al., 2007; Meima et al., 2009; Snabaitis et al., 2008; Takahashi et al., 1999).

In micropipette experiments, wild-type (wt) MEFs with primary cilia move chemotactically toward a gradient of PDGF-AA released from the pipette, while *Tg737*^{orpk} MEFs that form no or stunted cilia are blind to the gradient (Schneider et al., 2010). The primary cilia, oriented in the direction of movement, must detect the PDGF-AA gradient and via the PI3K–AKT and MEK1/2–ERK1/2 pathways relay this information to the cell. We hypothesize that after PI3K–AKT and MEK1/2–ERK1/2 activation in the PDGFRαα pathway, these signaling pathways exert their effect on NHE1 in part by controlling the spatial pathway and cytoskeletal structures along which the NHE1-containing vesicles move to the leading edge. Upon its insertion in the leading edge, NHE1 alkalinizes the cytoplasm and initiates a series of events pertinent to actin polymerization, lamellipodium formation and directional cell migration (Frantz et al., 2008; Magalhaes et al., 2011). In this way the direction in which the NHE1 containing vesicles travel to form the leading edge is specifically related to the orientation of the primary cilium.

To test this hypothesis, we investigated the function of PDGFRαα signaling in the primary cilium in coordinating NHE1 translocation and activation through the PI3K–AKT and MEK1/2–ERK1/2 pathways during cell migration in quiescent fibroblasts. We show that stimulation of ciliary PDGFRαα signaling leads to activation of p90^{RSK} downstream of MEK1/2–ERK1/2, independently of AKT, and we demonstrate that p90^{RSK} is localized to the primary cilium and activated at the ciliary basal region after stimulation with PDGF-AA. Inhibition of either AKT or the MEK1/2–ERK1/2–p90^{RSK} axis inhibited cell migration, but we find that this occurs by two distinct mechanisms: AKT inhibition reduced the formation of focal adhesions and blocked the translocation of NHE1 to the leading edge cell membrane, concomitant with reduced NHE1 activity as measured by changes in the rate of intracellular pH (pH_i) recovery after acidification. In contrast, MEK1/2 inhibition did not affect NHE1 activity, but elicited the formation of multiple and uncoordinated cell extensions and loss of a well-defined leading edge. Further, in MEK1/2-inhibited cells, the spatial organization of microtubule (MT) bundles and focal adhesions was disrupted in parallel with a loss of stress fiber organization, and NHE1 localized more broadly in various regions along the plasma membrane, rather than preferentially to the cell edges facing toward the wound. These results suggest that PDGFRαα signaling regulates cell migration differentially through the AKT and the MEK1/2–ERK1/2–p90^{RSK} pathways, with the AKT pathway necessary to initiate NHE1 translocation to the leading edge, while the MEK1/2 pathway controls the spatial organization of NHE1 translocation and incorporation and therefore specifies the direction in which the leading edge forms.

Results

PDGF-AA activates p90^{RSK} at the primary cilium downstream of MEK1/2–ERK1/2 pathway in NIH3T3 cells

To investigate the roles of the AKT and MEK1/2–ERK1/2 pathways in activation of p90^{RSK} and as well as in NHE1 activation and localization to the leading edge in migrating cells, we initially performed western blot (WB) analysis of activation of PDGFRαα [phosphorylation of tyrosine in position 754, p-PDGFRα(Y^{754})], AKT [phosphorylation of serine in position 473, p-AKT(S^{473})], ERK1/2 [phosphorylation of threonine and tyrosine in positions 202 and 204, respectively, p-ERK1/2(T^{202},Y^{204})] and p90^{RSK} during PDGF-AA stimulation and in the presence and in the absence of inhibitors of AKT (Akti1/2) and MEK1/2 (U0126). Activation of p90^{RSK} was measured by phosphorylation on threonine in position T^{573} (T^{573}) (in the C-terminal kinase domain, phosphorylated by ERK1/2), threonine and serine in positions 359 and 363 (in the turn motif, phosphorylated by ERK1/2), respectively (T^{359},S^{363}), and serine in position 380 (S^{380}) (in the hydrophobic loop, autophosphorylated by the C-terminal kinase domain). As shown in Fig. 1A,B, PDGFRα was phosphorylated within 3 min of stimulation (10.31±2.91-fold increase in

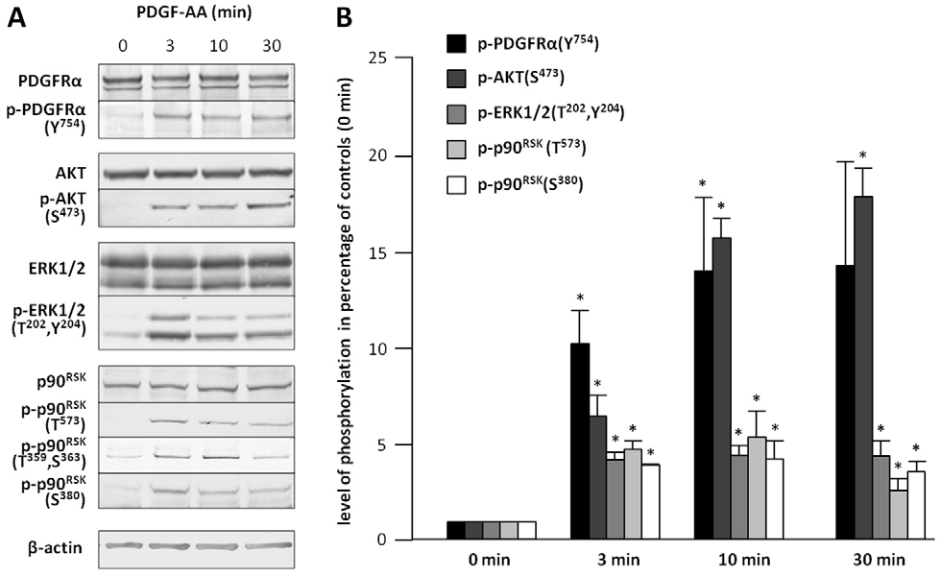

Fig. 1. Signaling pathways activated by PDGF-AA in NIH3T3 cells. (**A**) WB analysis of NIH3T3 cells after 24 h serum deprivation and stimulation with 25 ng/ml PDGF-AA for 0, 3, 10 or 30 min. Antibodies used were directed against total PDGFRα, Y754-phosphorylated PDGFRα, AKT, S473-phosphorylated AKT, ERK1/2, T202/Y204-phosphorylated ERK1/2, p90^{RSK}, T573-phosphorylated p90^{RSK}, T359/S363-phosphorylated p90^{RSK} and S380-phosphorylated p90^{RSK}; β-actin was used as a loading control. (**B**) Quantification of WB analysis and ANOVA ($n \geq 3$). The values at 0 min of stimulation were set to 1 and those at 3, 10 and 30 min of stimulation are the percentage phosphorylation compared to non-stimulated cells. *Significantly different from the respective control ($P<0.05$).

phosphorylation) and remained phosphorylated for at least 30 min. In the absence of inhibitors, the downstream effector molecules, AKT, ERK1/2 and p90^{RSK} showed a similar time course of activation [from t=0–10 min, p-AKT increased 6.51±1.75-fold, p-ERK1/2 increased 4.51±1.08-fold, p-p90^{RSK}(T^{573}) increased 5.45±2.17-fold and p-p90^{RSK}(S^{380}) increased 4.32±1.62-fold, see Fig. 1A,B]. These results confirm previous findings that ligand-dependent activation of PDGFRαα in the primary cilium is followed by activation of the PI3K–AKT and MEK1/2–ERK1/2 pathways (Schneider et al., 2005; Schneider et al., 2010). Further, we now show that these signaling events are coupled to activation of p90^{RSK}.

To analyze the roles of AKT and MEK1/2–ERK1/2 signaling upstream of p90^{RSK} activation in response to PDGFRαα signaling, Akti1/2 and U0126 were used to inhibit AKT and MEK1/2, respectively. WB was performed on NIH3T3 cells pre-incubated with Akti1/2 or U0126 for 1 h and subsequently stimulated with PDGF-AA for 10 min. As shown in Fig. 2A,B, phosphorylation of AKT is inhibited by Akti1/2 (0.1–10 µM) and phosphorylation of ERK1/2 is inhibited by U0126 (0.3–10 µM) in a dose-dependent manner, whereas Akti1/2 does not affect ERK1/2 phosphorylation and U0126 does not affect AKT phosphorylation. Further, p90^{RSK} S^{380} phosphorylation was unaffected by inhibition with Akti1/2 but reduced in a dose-dependent manner by U0126, with complete inhibition at 10 µM. The level of PDGFRα phosphorylation was unaffected by either inhibitors. Collectively, these results show that p90^{RSK} is activated downstream of the MEK1/2–ERK1/2 pathway in

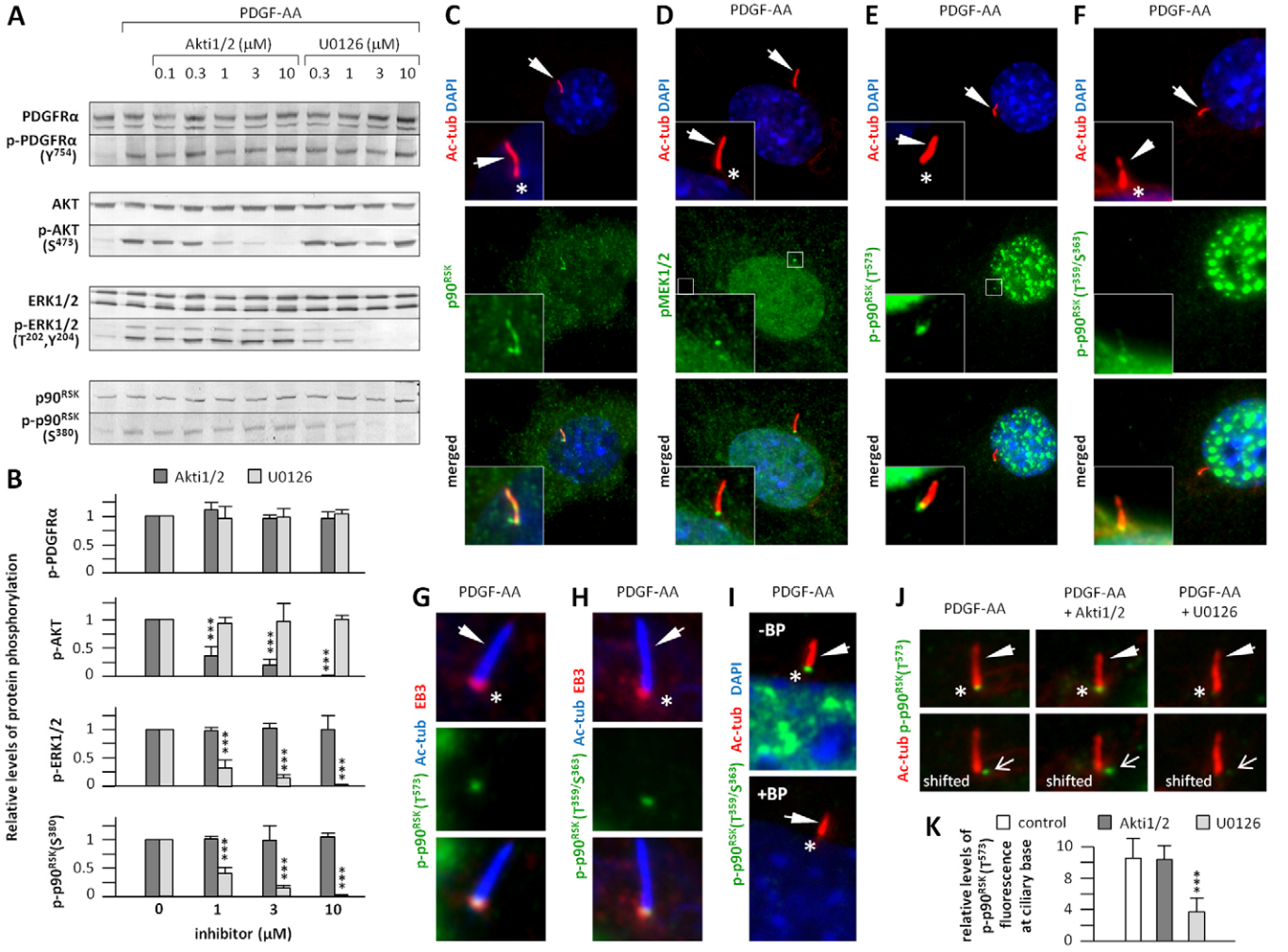

Fig. 2. p90RSK is activated by MEK1/2-ERK1/2 at the primary cilium. (**A**) WB analysis of the effects of the AKT inhibitor (Akti1/2: 0.1, 0.3, 1, 3, 10 µM, 1 h) and the MEK1/2 inhibitor (U0126: 0.3, 1, 3, 10 µM, 1 h) on PDGF-AA-mediated signal transduction in growth-arrested NIH3T3 cells. PDGF-AA was added at 25 ng/ml for 10 min. (**B**) Quantification of WB analysis and ANOVA (n=3). The inhibition of AKT by Akti1/2, and ERK1/2 and RSK by U0126 is considered extremely significant (***P<0.001). (**C–F**) IFM analysis of primary cilia after 24 h of serum starvation. 'PDGF-AA' indicates that cells were stimulated with the ligand for 10 min (25 ng/ml). Phospho-MEK1/2 (pMEK1/2), p90^{RSK} and phospho-p90^{RSK} (p-p90^{RSK}) are green; anti-acetylated α-tubulin (Ac-tub; in red) marks stable microtubules, including primary cilia (arrows). Nuclei were stained with DAPI (blue). (**G**,**H**) Cells were stimulated with PDGF-AA (25 ng/ml for 10 min) followed by IFM analysis to confirm localization of phospho-p90^{RSK} at the ciliary base. Primary cilia are marked with Ac-tub (blue, arrows) and centrosomes with anti-EB3 (red, asterisks); p-p90^{RSK} is green. (**I**) Cells without and with blocking peptide against p-p90^{RSK}(T^{573}). (**J**) Cells were pre-incubated for 1 h with either 10 µM U0126 or Akti1/2 followed by stimulation with PDGF-AA (25 ng/ml for 10 min) and IFM analysis. Primary cilia are marked with Ac-tub (red, arrows); p-p90^{RSK} is green (open arrows). The lower row of panels show shifted images, where p-p90^{RSK} is shifted to the right. (**K**) Quantification of relative p-p90^{RSK} fluorescence levels at the base of the cilia, from the cells shown in J. Reduced localization of p-p90^{RSK} fluorescence at the base of the cilia in the presence of U0126 is extremely significant (***P<0.001; ANOVA; n=30).

PDGFRα signaling, independently of AKT activity, supporting the conclusion that the inhibitors Akti1/2 and U0126 are pathway specific.

In order to determine the localization pattern of total and phosphorylated $p90^{RSK}$ after PDGF-AA stimulation of growth-arrested NIH3T3 cells, we next performed immunofluorescence microscopy (IFM) analysis. In the unstimulated cells, $p90^{RSK}$ localizes to the base and along the entire length of the primary cilium (Fig. 2C), as well as throughout the cytoplasm. In the presence of PDGF-AA, MEK1/2 was phosphorylated at the ciliary base, as expected (Schneider et al., 2005) (Fig. 2D) and phosphorylated $p90^{RSK}$ [p-$p90^{RSK}$(T^{573}) and p-$p90^{RSK}$(T^{359},S^{363})] also localized strongly to the ciliary base region, as well as to multiple spots throughout the nucleus (Fig. 2E,F). To confirm localization of phosphorylated $p90^{RSK}$ at the ciliary base, cells were triple labeled with anti-EB3 that localizes to the centrosome (Schrøder et al., 2011), showing that EB3 colocalizes with p-$p90^{RSK}$(T^{573}) and p-$p90^{RSK}$(T^{359},S^{363}) (Fig. 2G,H). In some cases, both MEK1/2 and $p90^{RSK}$ phosphorylations were observed along the cilium, suggesting transport of the activated proteins from the cilium to the base. Previous studies by us and others have shown that $p90^{RSK}$ localizes to the nucleus, nuclear membrane region, and cytoplasm (e.g. Anjum and Blenis, 2008; Gorbatenko et al., 2011), but this is the first study to report its localization at the primary cilium. Confirming the specificity of binding, pre-incubation of the anti-p-$p90^{RSK}$(T^{359},S^{363}) antibody with the corresponding blocking peptide removed the anti-p-$p90^{RSK}$(T^{359},S^{363}) labeling both at the ciliary base region and in the nucleus (Fig. 2I). Because of differences in antibody sensitivity quantitation between ciliary base and nuclear localizations of phosphorylated $p90^{RSK}$ in IFM analysis is non-linear, so that in WB analysis, phosphorylations reflect primarily localization to the ciliary base. To confirm this, treatment of PDGF-AA-stimulated cells with U0126 but not Akti1/2 abolished $p90^{RSK}$ phosphorylation at the ciliary base (Fig. 2J,K). These results support the conclusion that $p90^{RSK}$ is activated downstream of the MEK1/2–ERK1/2 pathway after PDGFRαα signaling in the primary cilium, which results in activation of $p90^{RSK}$ at the ciliary base.

PDGF-AA-mediated activation of the PI3K–AKT and MEK1/2–ERK1/2–$p90^{RSK}$ pathways requires the formation of a primary cilium

In order to clarify the role of the primary cilium in activation of the PI3K–AKT and MEK1/2–ERK1/2–$p90^{RSK}$ pathways, WB analysis was carried out in growth-arrested wt and *Tg737*^{orpk} mouse embryonic fibroblasts (MEFs) in the presence and absence of Akti1/2 and U0126 (both at 10 μM) and in the presence and absence of PDGF-AA and PDGF-BB. *Tg737*^{orpk} MEFs have defects in the ciliary assembly machinery and therefore form very short (stunted) primary cilia (Fig. 3B). Consequently, signaling through PDGFRαα is blocked in *Tg737*^{orpk} MEFs (Schneider et al., 2005). Fig. 3A shows that in wt MEFs, phosphorylation of AKT, ERK1/2 and $p90^{RSK}$ is increased in the presence of PDGF-AA and inhibited by Akti1/2 and U0126 in a manner comparable to that seen in NIH3T3 cells (Fig. 1A,B). In wt MEFs, PDGF-BB stimulation produced an even stronger increase in the phosphorylation of AKT, ERK1/2 and $p90^{RSK}$ than did PDGF-AA, consistent with the known ligand function of PDGF-BB at both PDGFRαα and PDGFRββ in growth-arrested fibroblasts (Chen et al., 2012). In contrast, PDGF-AA-induced phosphorylation of AKT, ERK1/2 and $p90^{RSK}$ was abolished in *Tg737*^{orpk} mutant MEFs, whereas the phosphorylation levels of these proteins in the presence of PDGF-BB were comparable to those observed in wt cells. This supports our previous findings (Schneider et al., 2005; Schneider et al., 2010) that formation of a primary cilium is required for activation of PDGF-AA-mediated PDGFRαα signaling, whereas stimulation with PDGF-BB leads to AKT and MEK1/2–ERK1/2 activation independent of the cilium. Collectively, these results demonstrate that PDGFRαα-activation of AKT as well as of $p90^{RSK}$ via the MEK1/2–ERK1/2 pathway requires the formation of a primary cilium.

To further investigate the significance of ciliary PDGFRαα signaling in activation of $p90^{RSK}$ [p-$p90^{RSK}$($T^{359/}S^{363}$)], IFM analysis was carried out in wt and *Tg737*^{orpk} MEFs in the presence of PDGF-AA (Fig. 3C). As in NIH3T3 cells, activated $p90^{RSK}$ was observed in the nucleus as well as at the ciliary base of wt MEFs. Activated $p90^{RSK}$ was also observed in the nucleus of *Tg737*^{orpk} mutant MEFs at a level comparable to that of wt MEFs, but it was greatly decreased at stunted primary cilia (Fig. 3D). These results validate the finding that PDGFRαα signaling activates $p90^{RSK}$ at the primary cilium.

The roles of AKT and MEK1/2-dependent pathways in PDGF-AA-stimulated NIH3T3 cell migration

In order to investigate the roles of the AKT- and MEK1/2-dependent pathways in PDGF-AA mediated cell migration and localization of NHE1 to the leading edge, we performed scratch assays in the presence and absence of PDGF-AA and inhibitors of AKT, MEK1/2 and NHE1 in growth-arrested NIH3T3 cells. Fig. 4A shows trajectories of individual cells migrating into the wound normalized to a common starting point. The diagrams are based on cell migrations from scratch assays illustrated in Fig. 4C by differential interference contrast microscopy (DIC) and IFM analysis. The radii of the red circles represent the mean distances covered within 4 h of migration. Fig. 4B provides a statistical summary of these experiments. In the presence of PDGF-AA, cells migrated nearly twice as far as in the absence of the ligand (16.4±9.3 μm versus 29.0±16.7 μm), showing that PDGF-AA stimulates migration of quiescent NIH3T3 cells, as previously reported (Schneider et al., 2009; Schneider et al., 2010). After treatment with either U0126 or Akti1/2, the migration distance in PDGF-AA-stimulated cells was reduced to a level similar to that of control cells not treated with PDGF-AA (12.1±7.7 μm and 11.1±8.6 μm, respectively). When treated with both U0126 and Akti1/2, PDGF-AA-stimulated cells migrated on average 8.3±5.1 μm during the 4 h time course of the experiment. When NHE1 activity is inhibited by EIPA, cells migrated 8.8±4.4 μm, i.e. the effect of EIPA is comparable to the effect of combined AKT and MEK1/2 inhibition. In the presence of all three inhibitors, PDGF-AA-induced translocation was reduced to 6.6±3.2 μm. These results indicate that both AKT and MEK1/2-dependent pathways are critical elements leading from ciliary PDGFRαα signaling to induce cell migration, and that NHE1 activation is not additive to, but most likely downstream of, these pathways.

In order to investigate how AKT and MEK1/2-dependent pathways may contribute to lamellipodium formation and NHE1 trafficking to the leading edge of migrating cells, IFM analysis was carried out in scratch assays. Cells were stimulated with PDGF-AA and stained for NHE1 (anti-NHE1), F-actin (Alexa Flour®350 phalloidin), and microtubules (anti-α-tubulin) in growth-arrested NIH3T3 cells (Fig. 4C; supplementary material Fig. S1). Under control conditions, cells formed regular

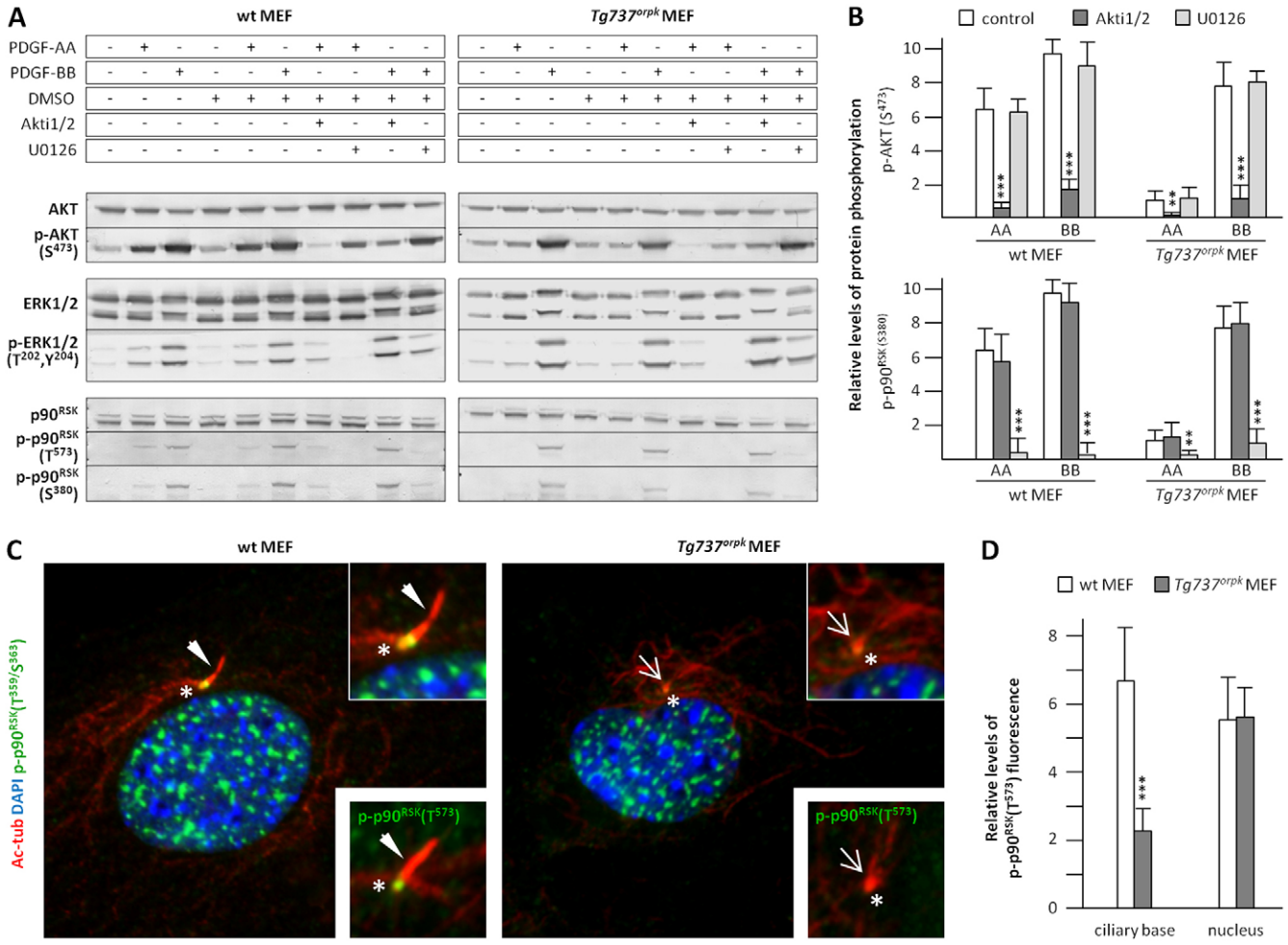

Fig. 3. PDGF-AA-mediated activation of the PI3K-AKT and MEK1/2-ERK1/2-p90RSK pathways is abolished at stunted primary cilia in *Tg737orpk* MEFs. (**A**) WB analysis after 24 h of serum deprivation of wt and *Tg737*^{orpk} MEF cells stimulated with or without PDGF-AA and PDGF-BB. Control cells are incubated with DMSO. (**B**) Quantification of WB analysis and ANOVA ($n=3$). The inhibition of AKT by Akti1/2, and ERK1/2 and p90RSK by U0126 is either very significant (**$P<0.01$) or extremely significant (***$P<0.001$). (**C**) IFM analysis of wt and *Tg737*^{orpk} MEFs with antibodies against anti-acetylated α-tubulin (Ac-tub, red), which marks stable microtubules, including primary cilia (arrows) and p-p90^{RSK}(T^{359}/S^{363}) (green). Nuclei were stained with DAPI (blue). Upper right inserts show magnifications of the ciliary base localization of p-p90^{RSK}(T^{359}/S^{363}). Lower right inserts show the ciliary base localization of p-p90^{RSK}(T^{573}) (green). Open arrows indicate stunted cilia in *Tg737*^{orpk} MEFs. Asterisks mark the base of a cilium. (**D**) Quantification of relative p-p90^{RSK} fluorescence levels at the base of the cilia from data shown in Fig. 2C. Reduced localization of p-p90^{RSK} fluorescence at the ciliary base in *Tg737*^{orpk} MEFs is extremely significant (***$P<0.001$; ANOVA; $n=30$).

lamellipodia in the direction of the wound, exhibiting the typical MT bundles extending from the nucleus to the lamellipodium and prominent cortical F-actin localization and clear leading edge NHE1 localization (left row of images). NHE1-labelled puncta (presumably NHE1-containing vesicles) were found throughout the cytoplasm but were very prominent at the leading edge. In Akti1/2-treated cells, there was a marked reduction in the projected area of lamellipodia towards the scratch, in congruence with the reduced cell translocation (Fig. 4A) under these conditions. Further, Akti1/2 treatment was associated with evident severing and loss of bundling of MTs, disruption of leading edge F-actin organization and loss of the preferential localization of NHE1 to the leading edge (Fig. 4C, middle row images; supplementary material Fig. S1). In U0126-treated cells (Fig. 4C, right row images; supplementary material Fig. S1), MT bundles seemed tighter but were multidirectional and F-actin organization per se seemed better preserved than in controls or after Akti1/2 treatment. These descriptions of cytoskeletal changes in actin organization as well as MT length and bundling are qualitative impressions from the IFM analysis and require future quantitative confirmation. The U0126-treated cells displayed no clear leading edge lamellipodia, but rather had multiple, apparently spatially uncoordinated protrusions. Interestingly and in contrast to the pattern seen in Akti1/2-treated cells, NHE1 localized to the cell membrane in U0126-treated cells, yet with a broad membrane distribution in several small distinct locations related to the protrusions, rather than preferentially along the smooth leading edge localization seen in controls. These results highlight major differences in the roles of AKT and MEK1/2–ERK1/2–p90^{RSK} pathways in ciliary PDGFRαα signaling to control changes in actin cytoskeleton and NHE1 translocation to the leading edge.

The extensive changes in lamellipodial structure in conjunction with the altered NHE1 translocation after Akti1/2

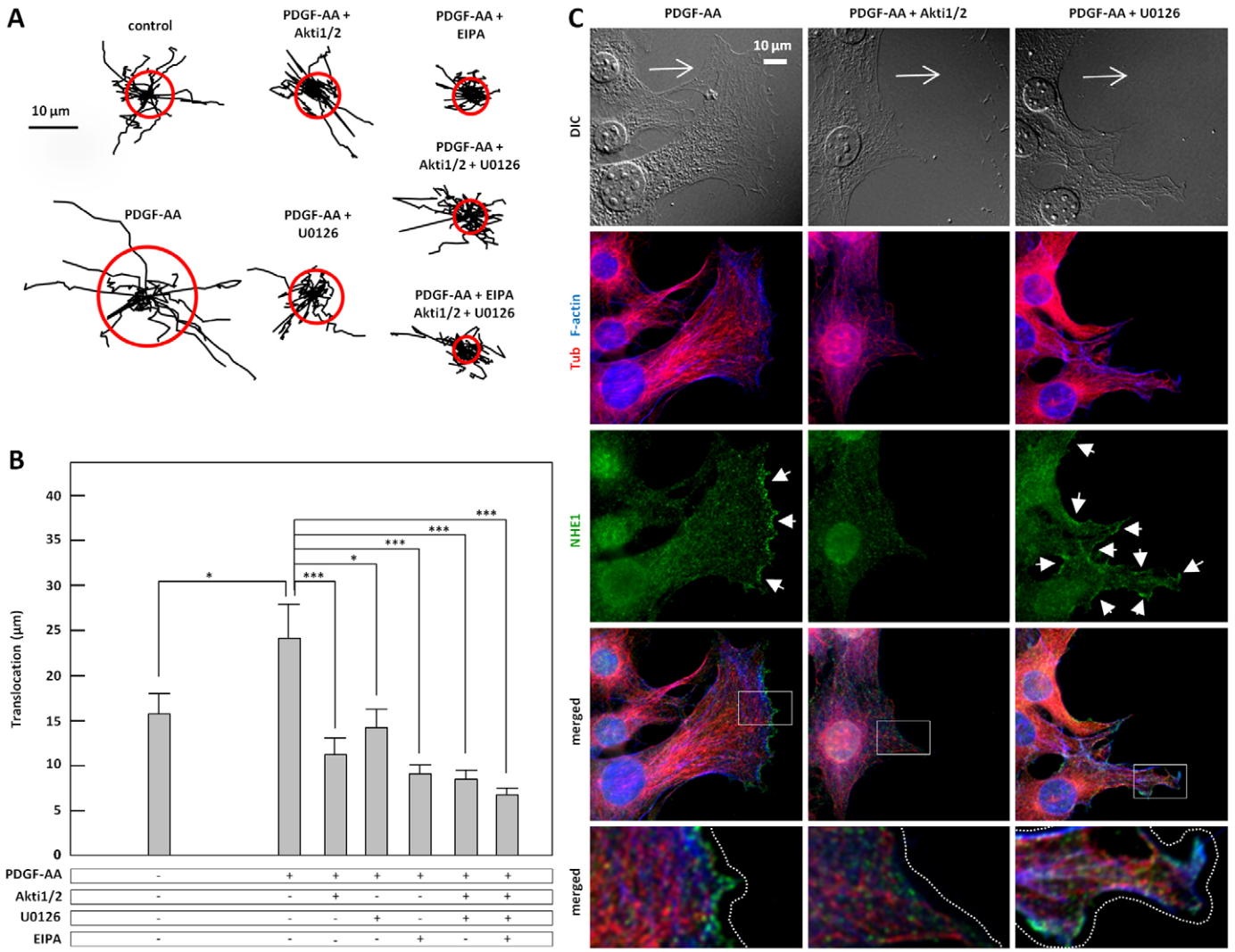

Fig. 4. Effects of PDGF-AA, Akti1/2, U0126 and EIPA in wound-healing and localization of NHE1 in growth-arrested NIH3T3 fibroblasts. (**A**) Wound healing assay trajectories of growth-arrested NIH3T3 cells. Each line represents the migration of one cell within a 4 h period. The red circles illustrate the mean translocation of the cells. (**B**) Translocation in the absence or presence of inhibitor (10 µM) and PDGF-AA (25 ng/ml) as indicated (ANOVA: $*P<0.05$; $***P<0.001$; $n=3$). (**C**) IFM analysis of cell culture with scratch after 24 h of serum starvation. Anti-α-tubulin (Tub, red) marks microtubules, the actin cytoskeleton is stained with phalloidin (F-actin, blue) and NHE1 is stained with anti-NHE1 (green, bold arrows). Differential interference contrast (DIC) images show the three-dimensional appearance. Open arrows indicate direction of migration into the scratch. The lowest row of panels shows magnifications of the boxed areas in the fourth row of merged images. The dotted lines indicate the surface of the cells facing the scratch.

and U0126 treatment are indicative of altered cell adhesion. We therefore next analyzed the cellular distribution of F-actin and NHE1 together with the focal adhesion marker vinculin in cells exposed to scratch assay conditions (Fig. 5). In PDGF-AA-treated control cells focal adhesions are abundant and associated with stress fiber endings visible as vinculin puncta in lamellipodia of migrating cells. This is in sharp contrast to cells treated with Akti1/2, where no clear vinculin puncta were observed. This suggests that AKT regulates formation of both lamellipodia and focal contacts in PDGF-AA-stimulated cells such that AKT inhibition leads to aberrant stress fiber assembly and cell spreading in concurrence with disruption of leading edge F-actin and loss of NHE1 localization to the leading edge (Figs 4, 5). In U0126-treated cells, vinculin puncta were readily observed, but their spatial organization appeared to be disrupted compared to that in PDGF-AA-treated controls, in accordance with the altered stress fiber organization. Collectively, these results indicate that AKT and MEK1/2 signaling in response to ciliary PDGFRαα activation regulate cell migration by different mechanisms through effects on actin organization, focal contact formation, MT bundle formation, and translocation of NHE1-containing vesicles to the leading edge.

Intracellular NHE1–GFP transport and incorporation at the leading edge

In order to confirm the differential effects of Akti1/2 and U0126 on the translocation of NHE1 to the leading edge, we stably transfected wt MEFs with NHE1 C-terminally tagged with GFP. WB analysis confirmed that NHE1–GFP is expressed in transfected cells, with NHE1–GFP (~135 kDa) being

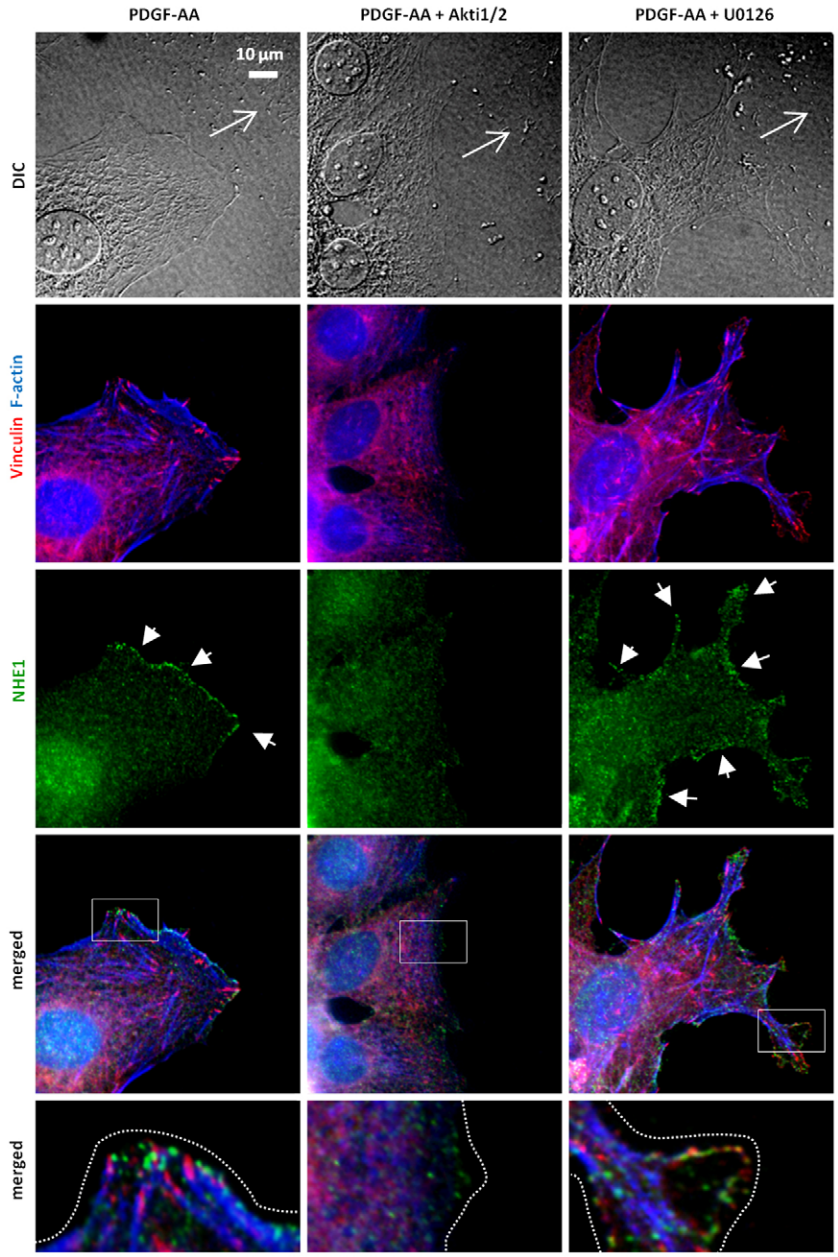

Fig. 5. Effects of Akti1/2 and U0126 on focal contact formation and NHE1 localization during wound healing in growth-arrested NIH3T3 fibroblasts. IFM analysis of NIH3T3 cell culture with scratch after 24 h of serum starvation with antibodies against vinculin (red) and NHE1 (green, bold arrows); the actin cytoskeleton is stained with phalloidin (F-actin, blue). DIC images show the three-dimensional appearance. Open arrows indicate direction of migration into the scratch. The lowest row of panels shows magnifications of the boxed areas in the fourth row of merged images. The dotted lines indicate the surface of the cells facing the scratch.

recognized by both anti-GFP and anti-NHE1, whereas endogenous NHE1 (~110 kDa) was recognized by anti-NHE1 only (Fig. 6A). The level of endogenous NHE1 increased during growth arrest after 24 h of serum starvation, as previously demonstrated (Schneider et al., 2009). The level of NHE1–GFP decreased during serum starvation, probably because of reduced promoter activity of the construct under these conditions.

Initially, cell migration was examined by time lapse video microscopy and DIC imaging (supplementary material Movie 1), in which NHE1–GFP is observed in the Golgi and in small puncta as the cell moves (supplementary material Movie 2). NHE1–GFP puncta often moved along linear paths into and out of developing lamellipodia, indicating vesicular trafficking of NHE1–GFP. The transfected MEFs were grown to confluency and serum starved for 24 h to form primary cilia. A scratch was made, PDGF-AA was added alone or with one of the inhibitors, and the cells at the wound edge were followed by video microscopy for 4 h. Subsequently, the cells were fixed for IFM analysis using anti-GFP. All preparations showed significant localization of NHE1–GFP to what appears to be the Golgi apparatus, and throughout the cytoplasm as small puncta (Fig. 6B). In cells treated with PDGF-AA alone, there was a gradient of NHE1–GFP localization from the Golgi outward, then localization to the leading edge appeared as a sharp bright line continuous along the broad lamellipodium (Fig. 6B, left panel). When Akti1/2-treated cells were exposed to PDGF-AA (Fig. 6B, middle panel), the gradient was less obvious, there was no clear lamellipodium and no NHE1–GFP localization was seen at the edge towards the scratch. In contrast, when U0126-treated cells were exposed to PDGF-AA, the single broad lamellipodium was replaced by multiple smaller protrusions, each with NHE1–GFP localization at the membrane edge (Fig. 6B, left panel). These observations

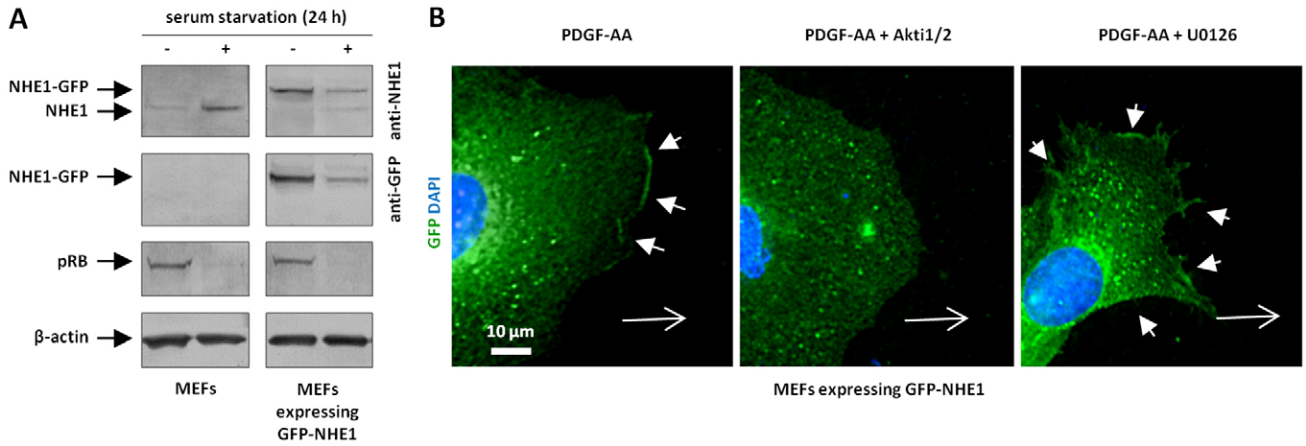

Fig. 6. Translocation of NHE1–GFP to the leading edge of migrating MEFs. (**A**) WB analysis of NHE1–GFP expression in non-transfected and stably expressing MEFs in cycling cells (+ serum) and in growth-arrested cells (− serum). (**B**) Effects of Akti1/2 and U0126 in scratch assays on localization of NHE1–GFP (green) in growth-arrested MEFs stimulated with PDGF-AA by IFM analysis. The NHE1–GFP signal was increased with anti-GFP. Open arrows indicate direction of movement into the scratch. Solid arrows indicate NHE1–GFP localization at the cell edges. The analysis was carried out in more than 30 transfected cells with similar result.

agree well with the findings on endogenous NHE1 localization under these conditions, reinforcing the conclusion that upon stimulation of PDGFRαα ciliary signaling by PDGF-AA, NHE1 is transported to the forming lamellipodium, and that AKT inhibition obliterates such transport, while MEK1/2 inhibition changes its cohesion via cytoskeletal reorganization.

NHE1 activity in NIH3T3 cells after inhibition of AKT and MEK1/2–ERK1/2–p90^{RSK} pathways

We have previously shown that NHE1 is activated by PDGF-AA stimulation of growth-arrested NIH3T3 cells (Schneider et al., 2009). However, these experiments were carried out in HEPES-buffered conditions that do not precisely reflect the *in vivo* conditions in migrating cells, in which CO_2/HCO_3^- buffering allows the additional contributions of HCO_3^--dependent pH regulatory transporters to total cellular pH regulation. To determine the impact of NHE1 on cellular pH regulation under CO_2/HCO_3^--buffered conditions and assess whether inhibition of AKT and MEK1/2–ERK1/2 signaling may alter cell motility in part via NHE1 inhibition, we carried out pH recovery assays in the presence of 25 mM HCO_3^-. The cells were acidified using the NH_4Cl prepulse technique (Boron, 2004; Roos and Boron, 1981), and the recovery from acidification monitored by BCECF fluorescence measurements. In PDGF-AA-treated control cells, the rate of pH_i recovery after acidification was 0.40±0.06 pH units/min (n=7). As seen from the effect of EIPA on pH_i recovery, the contribution of NHE1 is only about one-third of the pH_i recovery rate in PDGF-AA-treated cells under CO_2/HCO_3^--buffered conditions, in good agreement with the sizable contributions HCO_3^--dependent transporters to net acid extrusion seen in many cell types (Boedtkjer et al., 2012; Lauritzen et al., 2010; Lauritzen et al., 2012). U0126 pretreatment alone had no significant effect on pH_i recovery (Fig. 7A,C), whereas Akti1/2 pretreatment resulted in a significant decrease in the pH_i recovery rate, to 0.29±0.08 pH units/min (Fig. 7A,C). Interestingly, U0126 and Akti1/2 in combination strongly attenuated pH_i recovery, to 0.1±0.09 pH units/min, indicative of a synergistic effect (Fig. 7B,E). The further addition of EIPA did not reduce the recovery rate further; 0.11±0.1 pH units/min (Fig. 7B,E), supporting that AKT and/or MEK1/2–ERK1/2–p90^{RSK} may act upstream of NHE1 and/or other pH regulatory transporters. In conjunction with the inhibitory effect of Akti1/2 on NHE1 membrane localization demonstrated above, these data indicate that transport involving AKT activation is necessary for NHE1 activation and subsequent cytoplasmic alkalinization, and MEK1/2–ERK1/2 signaling inhibition by U0126 permits translocation and activation to proceed normally, even as directional co-ordination is disrupted. The synergistic inhibitory effect on pH_i recovery via both inhibitors suggests that other pH regulatory transporters downstream of PDGFRαα activation may also be affected.

Discussion

We previously showed that ciliary PDGFRαα signaling to the Na^+/H^+ exchanger NHE1 plays an essential role in directional fibroblast migration during wound healing (Schneider et al., 2009; Schneider et al., 2010). The role of NHE1 in cell migration is complex and differs between different cell types and stimuli. NHE1 regulates several aspects of cell migration, including integrin-mediated cell adhesion, matrix degradation and cytoskeletal dynamics, and at least the latter in both pH-dependent and -independent manners (for reviews see Meima et al., 2007; Pedersen et al., 2011). In this study, we attempt to clarify the mechanisms through which ciliary PDGFRαα signaling impacts on NHE1 activity and cell migration, and whether this is associated with regulation of NHE1 translocation to the leading edge of a migrating fibroblast.

Ciliary PDGFRαα signaling activates the MEK1/2–ERK1/2 effector p90^{RSK} in the ciliary base region

Although AKT and MEK1/2–ERK1/2 pathways can be activated by PDGF receptors in both the ciliary and non-ciliary cell membrane, the activation of PDGFRαα signaling requires the primary cilium. *Tg737*^{orpk} MEFs that form no or stunted cilia express PDGFRα, but the receptor cannot be activated following stimulation with PDGF-AA in these cells as judged by WB

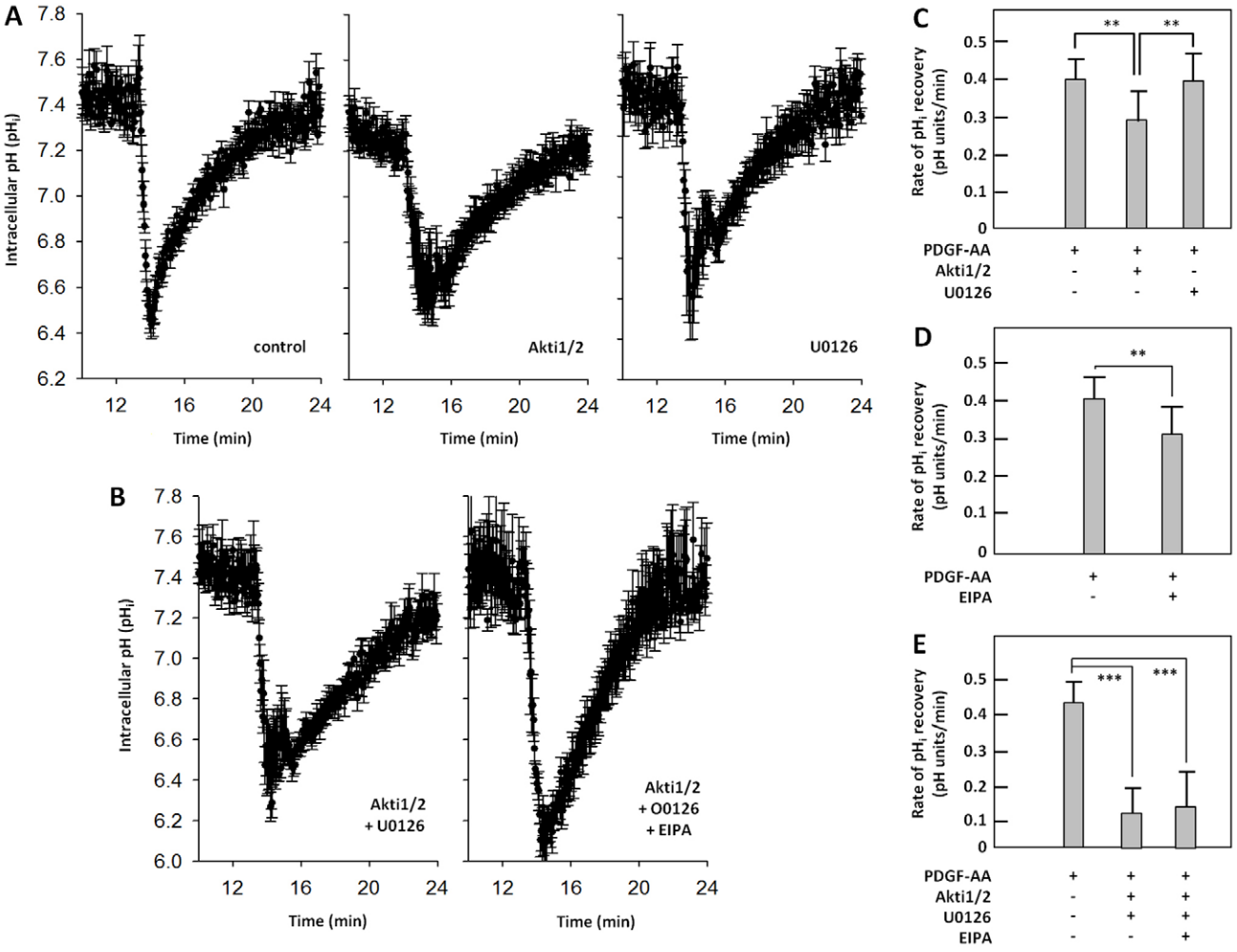

Fig. 7. Effects of MEK1/2, AKT and NHE1 inhibitors on intracellular pH recovery during growth arrest in NIH3T3 cells. (**A**,**B**) Tracings of pH_i recovery measurements after acidification and stimulation with PDGF-AA (25 ng/ml) and in the absence or (A) presence of Akti1/2 (10 μM) or U0126 (10 μM), and (B) Akti1/2+U0126 or Akti1/2+U0126+EIPA. (**C–E**) Summary of the pH_i recovery rates under the conditions shown. The rate of pH_i recovery (in pH units/minute) was calculated from the slope of the initial linear part of the curve after NH_4Cl removal. Data were analyzed using ANOVA: $^{**}P<0.01$ $^{***}P<0.001$ ($n=6$).

analysis, and chemotaxis toward a gradient of PDGF-AA is abolished in *Tg737*^{orpk} MEFs (Schneider et al., 2005; Schneider et al., 2010). We cannot rule out that a very small portion of PDGFRα is targeted to and incorporated into the plasma membrane in these cells or that a small amount is localized to stunted cilia, but the functional assays show that even if this is the case, there is not enough response to produce chemotaxis and directed cell migration. Therefore functional PDGFRαα signaling seems to be exclusively activated in the primary cilium.

We previously showed that AKT and MEK1/2–ERK1/2 are activated at the ciliary base region following PDGFRαα activation in the cilium (Schneider et al., 2005). Here, we show that ciliary PDGFRαα signaling is coupled to activation of the p90^{RSK} downstream of MEK1/2–ERK1/2. Further, we demonstrate that phosphorylated p90^{RSK} localizes to the base of the cilium. This localization of activated p90^{RSK} to the ciliary base region is dependent on the formation of a fully functioning primary cilium, as demonstrated by its absence in *Tg737*^{orpk} MEFs. In addition to its possible role in PDGFRαα-mediated NHE1 regulation (see below), this localization of activated p90^{RSK} in conjunction with the centrosome is likely to be important for the known role of p90^{RSK} in regulation of pathways controlling cell growth and cell cycle progression (Anjum and Blenis, 2008).

Cell migration stimulated by ciliary PDGFRαα signaling depends on AKT, MEK1/2 and NHE1

Our previous work (Schneider et al., 2009) demonstrated that inhibition of NHE1 strongly attenuates the PDGF-AA-induced translocation of NIH3T3 cells. We now show that inhibition of either AKT or MEK1/2 (to inhibit ERK1/2–p90^{RSK}) strongly attenuated cell migration. The simultaneous inhibition of both pathways was quantitatively indistinguishable from that of inhibition of NHE1, and the combined effect of inhibition of AKT, MEK1/2 and NHE1 was comparable to that of inhibition of AKT and ERK1/2 together, or NHE1 alone. In conjunction with our finding that pH_i recovery after acid loading is strongly attenuated by inhibition of AKT, this suggests that NHE1 activation by PDGF-AA is downstream from AKT signaling, in agreement with previous findings that NHE1 stimulation by

PDGF in fibroblasts is dependent on PI3K–AKT signaling (Meima et al., 2009). The lack of inhibition of net cellular NHE1 activity after inhibition by U0126 suggests that the effect of the MEK1/2 pathway on motility is not linked to global cellular NHE1 activity; however, altered local activity at the leading edge remains a possibility.

AKT and MEK1/2 pathways act differentially on cytoskeletal rearrangement and on the transport of NHE1 to the leading edge

We previously showed that NHE1 localizes to the plasma membrane after 1 h of PDGF-AA stimulation in *Tg737*^{orpk} MEFs (Schneider et al., 2009). In Tg737 MEFs, basic AKT and MEK1/2 activity is almost unaffected by PDGF-AA stimulation (Fig. 3B,C). This residual activity is therefore minimally related to PDGFRα signaling, but is still Akti1/2 and U0126 inhibitable. Thus, the most likely explanation is that this residual AKT and MEK1/2 activity partially maintains NHE1 in the leading edge plasma membrane of the mutant cells, to an extent that did not allow us to detect a difference between mutant and wt MEFs after 1 h of PDGF-AA stimulation (Schneider et al., 2009). In the present study, completely abolishing AKT and MEK1/2 activity in wt MEFs by using the inhibitors exacerbated the turnover in NHE1 localization, so that by 4 h there were remarkable differences at the leading edge, with and without inhibitors in wt cells. Tg737 mutants have not yet been studied in a comparable manner.

A pertinent finding of the present study is that NHE1 is translocated to the leading edge in an AKT-dependent manner during PDGF-AA-induced cell migration. This is in congruence with findings in cardiomyocytes, in which insulin stimulation induced PI3K-dependent NHE1 translocation to the plasma membrane (Lawrence et al., 2010). This conclusion is supported by both immunofluorescence imaging and by the studies of NHE1-GFP-transfected MEFs, where upon PDGF-AA stimulation; AKT inhibition attenuates intracellular transport of NHE1–GFP toward the leading edge and compromises lamellipodium formation, possibly by preventing NHE1–GFP vesicle delivery for exocytosis. When AKT is not inhibited, parallel bundles of MTs are found between the basal body of the primary cilium and the presumptive leading edge of the cell.

It is known that microtubule dynamics are essential for both cell polarization and migration in several cell types including fibroblasts (Gotlieb et al., 1983; Tanaka et al., 1995; Vasiliev et al., 1970). When NIH3T3 fibroblasts are treated with PDGF the amount of stabilized microtubules increases and this increase is abrogated by addition of a PI3K inhibitor or a dominant-negative form of AKT (Onishi et al., 2007). Upon AKT inhibition, possibly because the MT cytoskeleton is disrupted, the NHE1–GFP gradient disappears; NHE1–GFP puncta are found uniformly throughout the cytoplasm and little translocation is seen. A more complete analysis of vesicle movement will probably require super-resolution microscopy.

The mechanism of AKT-dependent NHE1 translocation to the leading edge remains to be determined. AKT has been shown to directly phosphorylate NHE1 on serine in position 648 (S^{648}) (Meima et al., 2009; Snabaitis et al., 2008; Takahashi et al., 1999) and in fibroblasts, this was associated with NHE1 activation (Meima et al., 2009). Furthermore, it is known that AKT-mediated phosphorylation of the Ral GAP complex (RGC) is involved in the activation of Ral (a central component of the exocyst complex), which in turn is essential for exocytosis of cell-surface proteins and thus for cell polarization (Chen and Saltiel, 2011; Wu et al., 2008). It is possible that Ral inhibition contributes to the AKT-inhibition-induced perturbation of NHE1 exocytosis and membrane localization. Further, membrane translocation of another NHE isoform, NHE5, is regulated by SCAMP2 in an Arf6-dependent manner (Diering et al., 2009). As Arf6 is also regulated by AKT signaling, via Grp1 (Li et al., 2012), it would also be relevant to address the possible role of this pathway in PDGF-αα-mediated NHE1 translocation. Both stimulatory and inhibitory roles of AKT on cell motility have been reported, possibly reflecting distinct roles of different AKT isoforms (for a review see Chin and Toker, 2009).

Although the ERK1/2 effector p90^{RSK} has been shown to activate NHE1 through direct phosphorylation on serine in position 703(S^{703}) (human NHE1 numbering) (Takahashi et al., 1999), MEK1/2 inhibition did not abrogate NHE1 activation after stimulation with PDGF or insulin (Meima et al., 2009). In agreement with this, we show here that pretreatment with U0126 did not inhibit NHE1 activation by PDGF-AA, nor did it abrogate cytoskeletal reorganization permitting delivery of NHE1 to the leading edge per se. However, inhibition of MEK1/2 seems to interfere with the formation of the normal parallel array of microtubule bundles along which NHE1–GFP vesicles could travel to form the leading edge lamellipodium. Instead, smaller MT bundles appeared to be splayed out from the Golgi in a variety of directions. Quantitative measurements of MT lengths and bundling after inhibitor treatment will be needed to confirm this analysis. In these cells, NHE1–GFP remained localized to the plasma membrane, yet failed to concentrate specifically to the leading edge, possibly because NHE1–GFP vesicles moved along the splayed MT bundles and exocytosed at discontinuous irregular spots along the membrane.

Local NHE1 accumulation in the leading edge or in invadopodia of migrating cells has previously been shown to regulate cytoskeletal organization. In the leading edge, several mechanisms were proposed, including ERM protein organization (Denker and Barber, 2002), and regulation of Cdc42 (Frantz et al., 2007). In invadopodia, NHE1-mediated local alkalinization was proposed to induce the release of cortactin-bound cofilin, resulting in F-actin barbed end generation and thus increased polymerization (Magalhaes et al., 2011). Where both AKT and MEK1/2–ERK1/2–p90^{RSK} pathways are activated after PDGF-AA addition, the continuous cortical actin network that participates in directed cell movement can be found immediately below the leading edge lamellipodium and vinculin puncta indicative of mature focal contacts appear in conjunction with the actin fibers. As expected, we found that the actin network and focal contacts are perturbed after AKT inhibition. Our data furthermore show that after U0126 addition, a single consolidated leading edge lamellipodium fails to form and is replaced with discontinuous NHE1 patches, actin polymerization and focal contact formation become irregular and F-actin spikes appear.

A novel finding of the present study is that AKT and MEK1/2–ERK1/2–p90^{RSK} pathways play important, and distinct, roles in lamellipodia formation and localization of NHE1 to the leading edge in response to PDGFR-αα activation. While clearly the direction in which the lamellipodium forms depends on normal MEK1/2 pathway activation, it is also related to the direction in which the primary cilium points during cell migration. How the

primary cilium direction influences cytoskeletal organization is unknown. One possibility could be that activation and/or localization of molecules such as AKAP450 and GM130 (Rivero et al., 2009) and therefore MT nucleation becomes asymmetric around the cilium. However, this model may be too simplistic and likely, multiple mechanisms are involved. ERK1/2-dependent mechanisms play roles in PDGF-AA-mediated NIH3T3 cell migration independent of their effects on NHE1 translocation. Thus, ERK1/2 is known to phosphorylate several proteins involved in cell migration and motility, including MLCK, FAK and calpain (Huang et al., 2004). The ERK1/2 effector $p90^{RSK}$ has been shown to regulate cell motility via, e.g. its regulation of filamin A (Rivero et al., 2009), and $p90^{RSK}$ activation also enhances motility through inhibition of the RhoA/Rock pathway by activation of $p27^{Kip1}$ (Larrea et al., 2009). Furthermore, $p90^{RSK}$ has been found to regulate cell motility via gene-regulatory mechanisms (Doehn et al., 2009), although such mechanisms may not be important within the relatively short time frame of the motility assays carried out in the present study.

In conclusion, signals derived from the primary cilium in the PDGFRαα cascade reorganize the cytoskeleton to permit directional cell migration, in large measure via transport of NHE1 to the forming leading edge lamellipodium. Signaling via AKT seems crucial for initiating NHE1 transport and activation, but the precise localization of NHE1 in the leading edge is dependent on the MEK1/2–ERK1/2 pathway. The exact mechanisms for generating asymmetry of NHE1 localization and hence activity, so that the leading edge forms and the cell moves in the direction in which the cilium points remain unknown, but presumably will be resolved by a further dissection of cell biological and cytoskeletal events downstream from the two pathways.

Materials and Methods

Cell cultures

Experiments were performed on NIH3T3 fibroblasts, wild-type (wt) and *Tg737*^{orpk} mutant MEFs. Tg737 encodes the protein polaris/IFT88, which is part of the intraflagellar transport protein complex responsible for assembly and maintenance of the primary cilium (Rosenbaum and Witman, 2002), thus *Tg737*^{orpk} MEFs form no or stunted primary cilia (Schneider et al., 2005). NIH3T3 cells were grown in DMEM (Invitrogen) with 10% fetal calf serum (Invitrogen) and 1% penicillin-streptomycin (Invitrogen). MEFs were grown in 50% DMEM and 50% F12 Ham (Invitrogen) with 10% fetal calf serum and 1% penicillin-streptomycin. All cells were maintained at 37℃, 5% CO_2, and 95% humidity. Cells were examined at either 70% confluency in the presence of serum (interphase cells) or at 90% confluency followed by serum starvation for 12 or 48 h to induce growth arrest and primary cilium formation. PDGF-AA and -BB (R&D Systems) stock solutions were prepared at 100 µg/µl in 4 mM HCl/0.1% BSA. 5′-N-ethyl-N-isopropyl-amiloride (EIPA) (Invitrogen) was prepared as a 5 mM stock in double-distilled H_2O, and BCECF-AM [2′,7′-bis-(2-carboxyethyl)-5,6-carboxyfluorescein, tetraacetoxymethylester; Invitrogen] as a 1.6 mM stock in desiccated DMSO. Akti-1/2 and U0126 (VWR) were prepared as 10 mM stock solutions in DMSO.

SDS-PAGE and western blot analysis

SDS-PAGE and western blotting (WB) was carried out essentially as previously described (Christensen et al., 2001). Cells were grown in Petri dishes, washed in ice-cold PBS and lysed with SDS lysis buffer. Cells were scraped off with a rubber policeman and briefly sonicated, followed by centrifugation for 5 min at 20,000 ***g***. The protein concentration was determined using a BioRad DC protein assay kit Protein BSA-standard king Reagent. Proteins were separated on 10% NuPAGE Bis-Tris gels by SDS-PAGE in an Xcell IITM Blot Module (Invitrogen) followed by transfer to a nitrocellulose membrane. The membranes were stained in 0.1% Ponceau S and incubated for 1 h in blocking buffer before incubation with primary antibody over night at 4℃. The antibodies used were: rabbit polyclonal anti-PDGFR-α (1:300; Santa Cruz Biotechnology, Inc.), rabbit polyclonal anti-phospho-Tyr754-PDGFR-α (1:100; Santa Cruz Biotechnology, Inc.), rabbit polyclonal anti-AKT (1:100; Cell Signaling), rabbit polyclonal anti-phospho-Ser473-AKT (1:200; Cell Signaling), rabbit polyclonal anti-p44/42 MAPK (ERK1/2) (1:100; Cell Signaling), rabbit polyclonal anti-phospho-Thr202/Tyr204-p44/42 MAPK (pERK1/2) (1:100; Cell Signaling), rabbit polyclonal anti–PDGFR-β (1:300; Santa Cruz Biotechnology, Inc.), rabbit polyclonal anti-phospho-Tyr857–PDGFR-β (1:1000; Santa Cruz Biotechnology, Inc.), rabbit polyclonal anti-$p90^{RSK}$-1 (1:100; Santa Cruz Biotechnology, Inc.), rabbit polyclonal anti-phospho-Ser380-$p90^{RSK}$ (1:100; Cell Signaling), rabbit polyclonal anti-phospho-Thr573-$p90^{RSK}$ (1:100; Cell Signaling), rabbit polyclonal anti-phospho-Thr359/Ser363-$p90^{RSK}$ (1:100; Santa Cruz), mouse polyclonal anti-β-actin (1:10,000; Sigma), mouse monoclonal anti-acetylated tubulin (1:5000; Sigma), mouse monoclonal anti-GFP (1:3000; Roche) and mouse monoclonal anti-NHE1 (1.1000; Chemicon). Finally, membranes were incubated with the relevant secondary alkaline-phosphatase-conjugated antibodies for 1 h at room temperature (1:5000 GAR, GAM; Sigma-Aldrich) and developed using BCIP/NBT. Band intensity was estimated from arbitrary densitometric values obtained with UN-SCAN-IT software.

Immunofluorescence microscopy analysis

Cells were grown on glass coverslips in six-well plates (Cellstar) and fixed with 4% paraformaldehyde in PBS for 15 min, followed by permeabilization in 0.2% Triton X-100 and blocking in PBS with 2% BSA for 30 min. Hereafter the cells were incubated with primary antibodies overnight at 4℃. Primary antibodies included mouse polyclonal anti-acetylated-α-tubulin (1:500; Sigma-Aldrich), rabbit polyclonal anti-$p90^{RSK}$ (1:100; Santa Cruz Biotechnology, Inc.), rabbit polyclonal anti-phospho-Thr359/Ser363-$p90^{Rsk}$ (1:100; Santa Cruz), rabbit polyclonal anti-phospho-Thr573-$p90^{Rsk}$ (1:100; Cell Signaling), rat polyclonal anti-EB3 (1:200; Absea), mouse monoclonal anti-vinculin (1:200; Sigma), mouse monoclonal anti-GFP (1:300; Roche) and rabbit polyclonal anti-NHE1 (1:50, Xb-17; a kind gift from M. Musch, University of Chicago, Chicago, IL). After primary antibody incubation, and washed in blocking buffer before incubation with secondary antibodies (1:600) for 45 min at room temperature (Alexa Flour®488 donkey anti-rabbit IgG, Alexa Flour®568 donkey anti-rat IgG, Alexa Flour®568 and Alexa Flour®350 donkey anti-mouse IgG, Molecular Probes). DNA was labeled with 4′,-diamidino-2-phenylindole, dihydrochloride (DAPI) to mark nuclei (1:1000; Molecular Probes) and Actin was labeled with Alexa Fluor®350 phalloidin (1:600; Molecular Probes). To investigate properties associated with cell migration, cells were grown to 100% confluence, serum starved and hereafter a scratch was made with a 10 µl pipette tip. To analyze the activation of PDGFRαα, the cells were incubated with 25 ng/ml PDGF-AA for 10 min before fixation. Preparations were mounted in *N*-propyl-gallate at 2% in PBS/glycerol and visualized with Nikon Eclipse E600, Olympus BX63 and inverted Olympus IX71 microscopes. Image acquisition was performed using an Optronics MagnaFire CCD, Olympus DP72 color CCD and Photometrics black and white EMCDD cameras. Image adjustments (overlays and contrast/brightness) were carried out in Adobe Photoshop. For quantification of fluorescence (Fig. 2K; Fig. 3D) images were analyzed with Olympus CellSens Dimension software and mean fluorescence values at the ciliary base were set relative to the fluorescence values in the background areas of the cytosol.

Cloning of NHE1-GFP and transfection of MEFs for transport studies

A NHE1-GFP construct (GFP at C-term of NHE1) was obtained, courtesy of Diane Barber, University of California San Francisco. The construct was fused at the 5′ end with the *Eco*RI site at the 3′ end of full length NHE1, and at the 3′ end with the *Sal*I site of pBabe puro. The resulting NHE1-GFP construct was cloned into the retroviral vector pQCXIP (Clontech cat. no. 631516). 293T cells were transfected using Lipofectamine together with the linked NHE1-GFP construct with p-VSV-G. The produced virus was collected and used for transduction of wt MEF cells. MEFs were transfected in the morning and again 8 h later for a total of 4 days. Stable transfectants were selected using an increasing gradient of puromycin and visualized by GFP fluorescence using a Deltavision system on an Olympus IX81 inverted microscope with a heated chamber (37℃). For initial studies designed to show NHE1–GFP transport within individual cells as they move, stably transfected cells were cultured to ~70% confluency in serum as above. 5×10^4 cells were transferred to a fibronectin coated coverslip. After 3 h, the medium was changed to imaging medium: six ml of Ham's F-12K without phenol red (Biosource), warmed to 37℃ to release dissolved gases. Argon gas was bubbled into medium for 1 min to displace oxygen. FCS was added (2% final) and mixed with Oxyfluor reagent (Oxyrase) at 1:100 dilution with 5 mM DL-lactate. The medium mixture was incubated at 37℃ for 1 h and spun down for 1 min at 24℃, 20,000 ***g***. Cells were placed in a custom-made chamber for imaging (Spiering and Hodgson, 2012) videotaped with a Olympus IX81 microscope for 2 h with a frame taken every minute using a Roper-Photometrics Coolsnap HQ2 camera.

Inhibitor assays

Cells at 80–90% confluence were serum-starved for 24–48 h and incubated for 1 h with the AKT inhibitor Akti-1/2 (VWR) or the MEK1/2 inhibitor U0126 (VWR), both dissolved in DMSO and at the concentrations indicated in the figures, before stimulating with PDGF-AA or PDGF-BB for 10 min. Controls were treated for 1 h with the corresponding amount of DMSO vehicle and were stimulated with the

buffer used to reconstitute PDGF-AA and -BB (sterile 4 mM HCl containing 0.1% BSA). Cells were lysed in lysis buffer followed by protein quantification and SDS-PAGE and WB analysis.

Migration assays

Cells were grown to 90% confluence and serum starved for 24 h. A wound was made by scraping with a sterile 10 µl pipette tip. The cells were allowed to recover for 1 h in 37℃ and 5% CO_2 before recording. Akti 1/2, U0126, and/or EIPA as indicated were added together with fresh medium 1 h before recording and PDGF-AA was added 10 min before recording. The flasks were sealed and placed in a heating chamber (37℃) on the stage of an inverted microscope (Axiovert 25 or Axiovert 40C; Zeiss, Oberkochen, Germany) at 10× or 32× magnification. To monitor 2D migration of the cells into the wound, pictures were taken every 5 min for 4 h with a Hamamatsu camera (Hamamatsu, Hersching, Germany) controlled by HiPic software (Hamamatsu Photonics). For evaluation of parameters (translocation distance, in µm), the circumferences of individual border cells were marked using Amira 5.2.2 software (TGS, France; http://www.amiravis.com/). Migration was quantified as the movement of the cell center per time unit, as previously described (Schneider et al., 2009). To analyze the localization of NHE1–GFP in migrating cell after wounding, cells stably transfected with NHE1-GFP were cultured to 90% confluency, serum starved and treated as above for IFM analysis with anti-GFP in order to increase the GFP signal.

Measurements of pH_i

pH_i was monitored at 37℃ essentially as previously described (Pedersen et al., 2007). In brief, NIH3T3 cells were seeded on glass coverslips 24 h before experiments. Confluency at the time of experiments was 80–95%. Cells were loaded with 1.2 µM BCECF-AM in Ringer's solution (125 mM NaCl, 25 mM $NaHCO_3$, 1 mM Na_2HPO_4, 1 mM $CaCl_2$, 10 mM HEPES, 5 mM glucose, pH 7.4), and mounted in the closed cuvette system of a spectrophotometer (Ratiomaster; PTI). Emission was detected at 525 nm after excitation at 445 and 495 nm. The 445:495 nm ratio was calculated after background subtraction, and calibration to pH_i was performed using the 7-point nigericin/high-K^+ technique, essentially as described by Boyarsky et al. (Boyarsky et al., 1988). The high-K^+ Ringer's solution was similar to the standard Ringer's solution, except that HCO_3^- was omitted and the Ringer's contained 140 mM KCl and 10 mM NaCl. The ability of the cells to recover after an acid load was evaluated by the NH_4Cl prepulse technique using (10 mM NH_4Cl in the Ringer's solution for 5 min) as previously described (Pedersen et al., 2007). The EIPA-dependent pH_i recovery is a measure of NHE1 activity. To estimate the contributions of AKT, MEK1/2 and NHE1, experiments were performed in the absence and presence of 10 µM Akti1/2 or U0126 and/or 5 µM EIPA, respectively. The effect of PDGF-AA was estimated by preincubating the cells with 25 ng/ml PDGF-AA for 1 h before the NH_4Cl prepulse. Because initial pH_i was comparable in all experiments, pH_i recovery was compared by calculating recovery rates (pH units/min) from the slope of the initial linear part of the curve after NH_4Cl removal.

Statistical analysis

All statistical calculations were performed by ANOVA. Data are shown as means ± s.e.m.; all experiments quantified were repeated three or more times independently of each other. The level of significance was set at $P<0.05$.

Acknowledgements

We thank Louis Hodgson for help with the GFP construct, transfection and initial video recording with this construct. We thank Anni Bech Nielsen for valuable technical expertise.

Funding

This work was supported by grants from the Lundbeck Foundation [grant numbers R54-A5642, R115-A10182 to S.T.C., P.S., respectively]; the Novo Nordisk Foundation [grant number R179-A15298 to S.T.C.]; the Danish National Research Foundation [grant numbers 10-085373, 09-070398 to S.T.C. and S.F.P.]; Nordforsk [grant number 27480 to S.T.C.]; and a Scandinavia Foundation fellowship to M.L.

Supplementary material available online at
http://jcs.biologists.org/lookup/suppl/doi:10.1242/jcs.116426/-/DC1

References

Anjum, R. and Blenis, J. (2008). The RSK family of kinases: emerging roles in cellular signalling. *Nat. Rev. Mol. Cell Biol.* **9**, 747-758.

Boedtkjer, E., Bunch, L. and Pedersen, S. F. (2012). Physiology, pharmacology and pathophysiology of the pH regulatory transport proteins NHE1 and NBCn1: similarities, differences, and implications for cancer therapy. *Curr. Pharm. Des.* **18**, 1345-1371.

Boron, W. F. (2004). Regulation of intracellular pH. *Adv. Physiol. Educ.* **28**, 160-179.

Boyarsky, G., Ganz, M. B., Sterzel, R. B. and Boron, W. F. (1988). pH regulation in single glomerular mesangial cells. II. Na+-dependent and -independent Cl(-)-HCO3-exchangers. *Am. J. Physiol.* **255**, C857-C869.

Chen, X. W. and Saltiel, A. R. (2011). Ral's engagement with the exocyst: breaking up is hard to do. *Cell Cycle* **10**, 2299-2304.

Chen, P. H., Chen, X. and He, X. (2012). Platelet-derived growth factors and their receptors: Structural and functional perspectives. *Biochim. Biophys. Acta* [Epub ahead of print] doi:10.1016/j.bbapap.2012.10.015.

Chin, Y. R. and Toker, A. (2009). Function of Akt/PKB signaling to cell motility, invasion and the tumor stroma in cancer. *Cell. Signal.* **21**, 470-476.

Christensen, S. T., Guerra, C., Wada, Y., Valentin, T., Angeletti, R. H., Satir, P. and Hamasaki, T. (2001). A regulatory light chain of ciliary outer arm dynein in Tetrahymena thermophila. *J. Biol. Chem.* **276**, 20048-20054.

Christensen, S. T., Pedersen, S. F., Satir, P., Veland, I. R. and Schneider, L. (2008). The primary cilium coordinates signaling pathways in cell cycle control and migration during development and tissue repair. *Curr. Top. Dev. Biol.* **85**, 261-301.

Christensen, S. T., Clement, C. A., Satir, P. and Pedersen, L. B. (2012). Primary cilia and coordination of receptor tyrosine kinase (RTK) signalling. *J. Pathol.* **226**, 172-184.

Denker, S. P. and Barber, D. L. (2002). Cell migration requires both ion translocation and cytoskeletal anchoring by the Na-H exchanger NHE1. *J. Cell Biol.* **159**, 1087-1096.

Denker, S. P., Huang, D. C., Orlowski, J., Furthmayr, H. and Barber, D. L. (2000). Direct binding of the Na–H exchanger NHE1 to ERM proteins regulates the cortical cytoskeleton and cell shape independently of H(+) translocation. *Mol. Cell* **6**, 1425-1436.

Diering, G. H., Church, J. and Numata, M. (2009). Secretory carrier membrane protein 2 regulates cell-surface targeting of brain-enriched Na+/H+ exchanger NHE5. *J. Biol. Chem.* **284**, 13892-13903.

Dixon, S. J., Cohen, S., Cragoe, E. J., Jr and Grinstein, S. (1987). Estimation of the number and turnover rate of Na+/H+ exchangers in lymphocytes. Effect of phorbol ester and osmotic shrinking. *J. Biol. Chem.* **262**, 3626-3632.

Doehn, U., Hauge, C., Frank, S. R., Jensen, C. J., Duda, K., Nielsen, J. V., Cohen, M. S., Johansen, J. V., Winther, B. R., Lund, L. R. et al. (2009). RSK is a principal effector of the RAS-ERK pathway for eliciting a coordinate promotile/invasive gene program and phenotype in epithelial cells. *Mol. Cell* **35**, 511-522.

Frantz, C., Karydis, A., Nalbant, P., Hahn, K. M. and Barber, D. L. (2007). Positive feedback between Cdc42 activity and H+ efflux by the Na-H exchanger NHE1 for polarity of migrating cells. *J. Cell Biol.* **179**, 403-410.

Frantz, C., Barreiro, G., Dominguez, L., Chen, X., Eddy, R., Condeelis, J., Kelly, M. J., Jacobson, M. P. and Barber, D. L. (2008). Cofilin is a pH sensor for actin free barbed end formation: role of phosphoinositide binding. *J. Cell Biol.* **183**, 865-879.

Goetz, S. C. and Anderson, K. V. (2010). The primary cilium: a signalling centre during vertebrate development. *Nat. Rev. Genet.* **11**, 331-344.

Gorbatenko, A., Wiwel, M., Klingberg, H., Nielsen, A. B., Kapus, A. and Pedersen, S. F. (2011). Hyperosmotic stress strongly potentiates serum response factor (SRF)-dependent transcriptional activity in Ehrlich Lettré Ascites cells through a mechanism involving p38 mitogen-activated protein kinase. *J. Cell. Physiol.* **226**, 2857-2868.

Gotlieb, A. I., Subrahmanyan, L. and Kalnins, V. I. (1983). Microtubule-organizing centers and cell migration: effect of inhibition of migration and microtubule disruption in endothelial cells. *J. Cell Biol.* **96**, 1266-1272.

Hildebrandt, F., Benzing, T. and Katsanis, N. (2011). Ciliopathies. *N. Engl. J. Med.* **364**, 1533-1543.

Huang, C., Jacobson, K. and Schaller, M. D. (2004). MAP kinases and cell migration. *J. Cell Sci.* **117**, 4619-4628.

Lagana, A., Vadnais, J., Le, P. U., Nguyen, T. N., Laprade, R., Nabi, I. R. and Noël, J. (2000). Regulation of the formation of tumor cell pseudopodia by the Na(+)/H(+) exchanger NHE1. *J. Cell Sci.* **113**, 3649-3662.

Larrea, M. D., Hong, F., Wander, S. A., da Silva, T. G., Helfman, D., Lannigan, D., Smith, J. A. and Slingerland, J. M. (2009). RSK1 drives p27Kip1 phosphorylation at T198 to promote RhoA inhibition and increase cell motility. *Proc. Natl. Acad. Sci. USA* **106**, 9268-9273.

Lauritzen, G., Jensen, M. B., Boedtkjer, E., Dybboe, R., Aalkjaer, C., Nylandsted, J. and Pedersen, S. F. (2010). NBCn1 and NHE1 expression and activity in DeltaNErbB2 receptor-expressing MCF-7 breast cancer cells: contributions to pHi regulation and chemotherapy resistance. *Exp. Cell Res.* **316**, 2538-2553.

Lauritzen, G., Stock, C. M., Lemaire, J., Lund, S. F., Jensen, M. F., Damsgaard, B., Petersen, K. S., Wiwel, M., Rønnov-Jessen, L., Schwab, A. et al. (2012). The Na+/H+ exchanger NHE1, but not the Na+, HCO3(-) cotransporter NBCn1, regulates motility of MCF7 breast cancer cells expressing constitutively active ErbB2. *Cancer Lett.* **317**, 172-183.

Lawrence, S. P., Holman, G. D. and Koumanov, F. (2010). Translocation of the Na+/H+ exchanger 1 (NHE1) in cardiomyocyte responses to insulin and energy-status signalling. *Biochem. J.* **432**, 515-523.

Li, J., Malaby, A. W., Famulok, M., Sabe, H., Lambright, D. G. and Hsu, V. W. (2012). Grp1 plays a key role in linking insulin signaling to glut4 recycling. *Dev. Cell* **22**, 1286-1298.

Magalhaes, M. A., Larson, D. R., Mader, C. C., Bravo-Cordero, J. J., Gil-Henn, H., Oser, M., Chen, X., Koleske, A. J. and Condeelis, J. (2011). Cortactin

phosphorylation regulates cell invasion through a pH-dependent pathway. *J. Cell Biol.* **195**, 903-920.

Malo, M. E., Li, L. and Fliegel, L. (2007). Mitogen-activated protein kinase-dependent activation of the Na+/H+ exchanger is mediated through phosphorylation of amino acids Ser770 and Ser771. *J. Biol. Chem.* **282**, 6292-6299.

Martin, C., Pedersen, S. F., Schwab, A. and Stock, C. (2011). Intracellular pH gradients in migrating cells. *Am. J. Physiol.* **300**, C490-C495.

Meima, M. E., Mackley, J. R. and Barber, D. L. (2007). Beyond ion translocation: structural functions of the sodium-hydrogen exchanger isoform-1. *Curr. Opin. Nephrol. Hypertens.* **16**, 365-372.

Meima, M. E., Webb, B. A., Witkowska, H. E. and Barber, D. L. (2009). The sodium-hydrogen exchanger NHE1 is an Akt substrate necessary for actin filament reorganization by growth factors. *J. Biol. Chem.* **284**, 26666-26675.

Onishi, K., Higuchi, M., Asakura, T., Masuyama, N. and Gotoh, Y. (2007). The PI3K-Akt pathway promotes microtubule stabilization in migrating fibroblasts. *Genes Cells* **12**, 535-546.

Patel, H. and Barber, D. L. (2005). A developmentally regulated Na-H exchanger in Dictyostelium discoideum is necessary for cell polarity during chemotaxis. *J. Cell Biol.* **169**, 321-329.

Pedersen, S. F. (2006). The Na+/H+ exchanger NHE1 in stress-induced signal transduction: implications for cell proliferation and cell death. *Pflugers Arch.* **452**, 249-259.

Pedersen, S. F., King, S. A., Nygaard, E. B., Rigor, R. R. and Cala, P. M. (2007). NHE1 inhibition by amiloride- and benzoylguanidine-type compounds. Inhibitor binding loci deduced from chimeras of NHE1 homologues with endogenous differences in inhibitor sensitivity. *J. Biol. Chem.* **282**, 19716-19727.

Pedersen, S. F., Lauritzen, G. and Andersen, A. D. (2011). *The Na^+/H^+ Exchanger NHE1*: *Diverse Roles in Regulation of Cellular Signaling Pathways Controlling Proliferation, Motility, and Survival.* pp. 13-28. Kerela, India: Research Signpost.

Rivero, S., Cardenas, J., Bornens, M. and Rios, R. M. (2009). Microtubule nucleation at the cis-side of the Golgi apparatus requires AKAP450 and GM130. *EMBO J.* **28**, 1016-1028.

Roos, A., Boron, W. F. (1981). Intracellular pH. *Physiol. Rev.* **61**, 296-434.

Rosenbaum, J. L. and Witman, G. B. (2002). Intraflagellar transport. *Nat. Rev. Mol. Cell Biol.* **3**, 813-825.

Satir, P., Pedersen, L. B. and Christensen, S. T. (2010). The primary cilium at a glance. *J. Cell Sci.* **123**, 499-503.

Schneider, L., Clement, C. A., Teilmann, S. C., Pazour, G. J., Hoffmann, E. K., Satir, P. and Christensen, S. T. (2005). PDGFRalphaalpha signaling is regulated through the primary cilium in fibroblasts. *Curr. Biol.* **15**, 1861-1866.

Schneider, L., Stock, C. M., Dieterich, P., Jensen, B. H., Pedersen, L. B., Satir, P., Schwab, A., Christensen, S. T. and Pedersen, S. F. (2009). The Na+/H+ exchanger NHE1 is required for directional migration stimulated via PDGFR-alpha in the primary cilium. *J. Cell Biol.* **185**, 163-176.

Schneider, L., Cammer, M., Lehman, J., Nielsen, S. K., Guerra, C. F., Veland, I. R., Stock, C., Hoffmann, E. K., Yoder, B. K., Schwab, A. et al. (2010). Directional cell migration and chemotaxis in wound healing response to PDGF-AA are coordinated by the primary cilium in fibroblasts. *Cell. Physiol. Biochem.* **25**, 279-292.

Schrøder, J. M., Larsen, J., Komarova, Y., Akhmanova, A., Thorsteinsson, R. I., Grigoriev, I., Manguso, R., Christensen, S. T., Pedersen, S. F., Geimer, S. et al. (2011). EB1 and EB3 promote cilia biogenesis by several centrosome-related mechanisms. *J. Cell Sci.* **124**, 2539-2551.

Snabaitis, A. K., Cuello, F. and Avkiran, M. (2008). Protein kinase B/Akt phosphorylates and inhibits the cardiac Na+/H+ exchanger NHE1. *Circ. Res.* **103**, 881-890.

Spiering, D. and Hodgson, L. (2012). Multiplex imaging of Rho family GTPase activities in living cells. *Methods Mol. Biol.* **827**, 215-234.

Stock, C. and Schwab, A. (2006). Role of the Na/H exchanger NHE1 in cell migration. *Acta Physiol. (Oxf.)* **187**, 149-157.

Takahashi, E., Abe, J., Gallis, B., Aebersold, R., Spring, D. J., Krebs, E. G. and Berk, B. C. (1999). p90(RSK) is a serum-stimulated Na+/H+ exchanger isoform-1 kinase. Regulatory phosphorylation of serine 703 of Na+/H+ exchanger isoform-1. *J. Biol. Chem.* **274**, 20206-20214.

Tanaka, E., Ho, T. and Kirschner, M. W. (1995). The role of microtubule dynamics in growth cone motility and axonal growth. *J. Cell Biol.* **128**, 139-155.

Vasiliev, J. M., Gelfand, I. M., Domnina, L. V., Ivanova, O. Y., Komm, S. G. and Olshevskaja, L. V. (1970). Effect of colcemid on the locomotory behaviour of fibroblasts. *J. Embryol. Exp. Morphol.* **24**, 625-640.

Wallingford, J. B. and Mitchell, B. (2011). Strange as it may seem: the many links between Wnt signaling, planar cell polarity, and cilia. *Genes Dev.* **25**, 201-213.

Waters, A. M. and Beales, P. L. (2011). Ciliopathies: an expanding disease spectrum. *Pediatr. Nephrol.* **26**, 1039-1056.

Wu, K. L., Khan, S., Lakhe-Reddy, S., Jarad, G., Mukherjee, A., Obejero-Paz, C. A., Konieczkowski, M., Sedor, J. R. and Schelling, J. R. (2004). The NHE1 Na+/H+ exchanger recruits ezrin/radixin/moesin proteins to regulate Akt-dependent cell survival. *J. Biol. Chem.* **279**, 26280-26286.

Wu, H., Rossi, G. and Brennwald, P. (2008). The ghost in the machine: small GTPases as spatial regulators of exocytosis. *Trends Cell Biol.* **18**, 397-404.

Yi, Y. H., Ho, P. Y., Chen, T. W., Lin, W. J., Gukassyan, V., Tsai, T. H., Wang, D. W., Lew, T. S., Tang, C. Y., Lo, S. J. et al. (2009). Membrane targeting and coupling of NHE1-integrinalphaIIbbeta3-NCX1 by lipid rafts following integrin-ligand interactions trigger Ca2+ oscillations. *J. Biol. Chem.* **284**, 3855-3864.

Journal of Cell Science

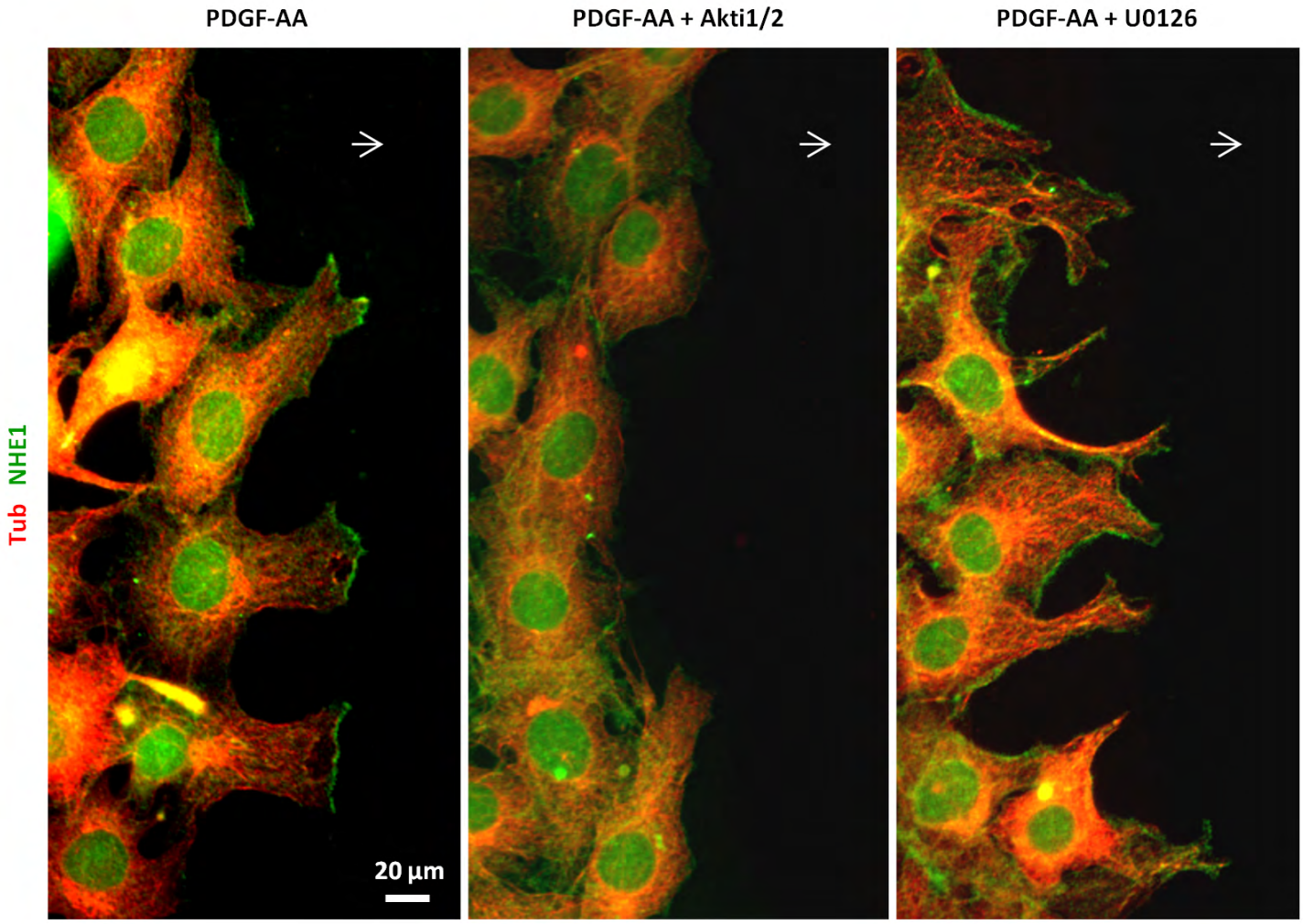

Fig. S1. IFM analysis of NIH3T3 cell culture with scratch after 24 h of serum starvation with antibodies against α-tubulin (red) and NHE1 (green). Open arrows indicate direction of migration into the scratch.

Movie 1. Live cell imaging by differential interference contrast (DIC) of wt MEFs stably expressing NHE1-GFP and taken with an Olympus IX81 microscope for 2 h with a frame taken every min using a Roper-Photometrics Coolsnap HQ2 camera.

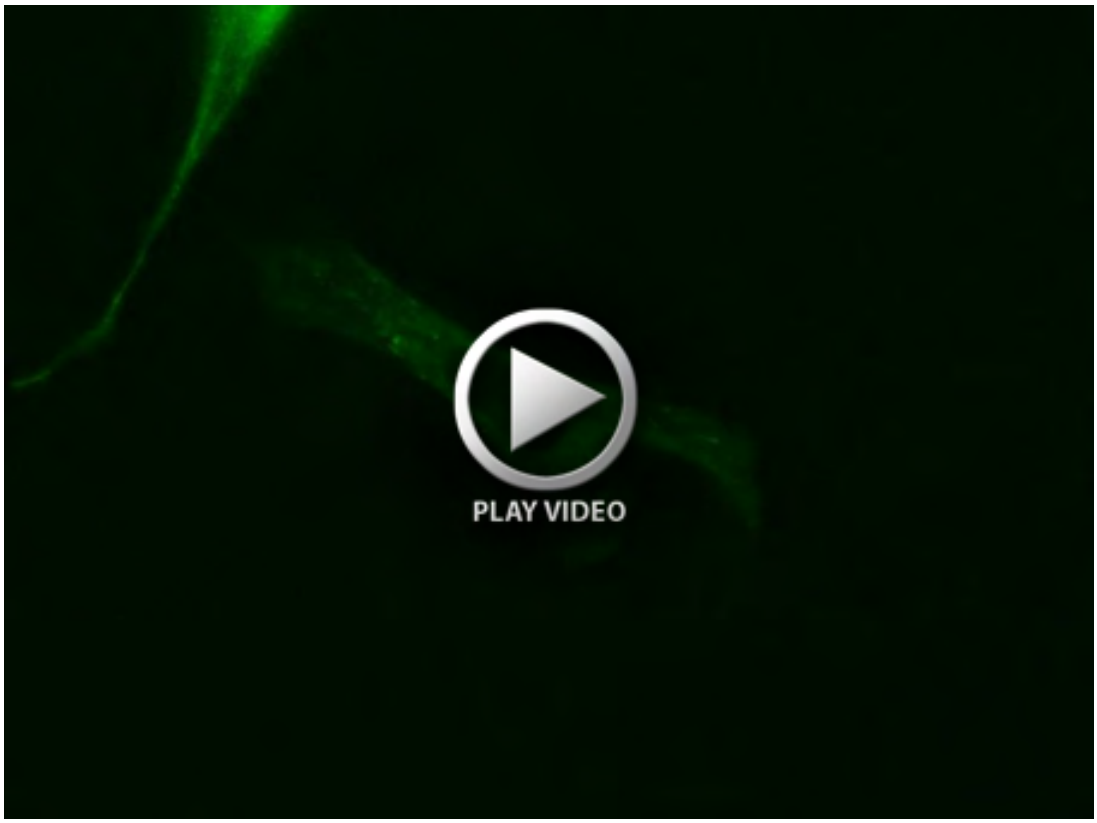

Movie 2. Live cell imaging by fluorescence microscopy of wt MEFs stably expressing NHE1-GFP (same cells as shown in Movie 1) and taken with an Olympus IX81 microscope for 2 h with a frame taken every min using a Roper-Photometrics Coolsnap HQ2 camera.